Computed SAR and Thermal Elevation in a 0.25-mm 2-D Model of the Human Eye and Head in Response to an Implanted Retinal Stimulator—Part II: Results

Gianluca Lazzi, *Senior Member, IEEE*, Stephen C. DeMarco, Wentai Liu, *Senior Member, IEEE*, James D. Weiland, *Member, IEEE*, and Mark S. Humayun, *Member, IEEE*

Abstract—This is the second of a series of two papers on the thermal increase in the human eye and head in response to an implanted retinal stimulator. This paper provides specific absorption rates induced in the human head by the extraocular unit and the temperature increases associated with induced electromagnetic fields and power dissipation of the implanted microchip. Results are provided for different assumptions about choroid blood flow. It is shown that computed results associated with the power dissipation of the implanted microchip, corresponding to temperature increases of approximately 0.6 °C in the midvitreous of the eye and 0.2 °C in the retina, closely parallel in-vivo experimental results in animals.

Index Terms—Age-related macular degeneration, finite-difference time domain (FDTD), retina prosthesis, retinitis pigmentosa, specific absorption rate (SAR), stimulator IC, temperature, thermal simulation.

I. INTRODUCTION

THE specific absorption rate and the dissipated stimulator IC power are the mechanisms that are expected to account for the ocular heating. Therefore, the numerical finite-difference time-domain (FDTD) method for specific absorption rate (SAR) computation and the numerical thermal method in Part I are applied to the newly developed truncated head/eye model to estimate the increase in temperature. In order to gain further insight into the results, the influence of SAR and dissipated power in the implant are considered separately.

II. SPECIFIC ABSORPTION RATE (SAR)

In a typical application of North Carolina State University's *Retina-3.5* microstimulator [1], in which it is assumed that the implant is operating with all channels active at current levels 100% of maximum specifications, required continuous supply currents of 10 mA were predicted. Experiments with inductive coupling based on the work in [2] showed that a power

of 200 Vpp at 2 A in the primary coil was necessary to obtain 10 mA of source current at $V_{dd} = 5$ v and $V_{ss} = -5$ v on the secondary side (power receiving coil). Therefore, the SAR distribution resulting from the numerical FDTD at 2 MHz has been linearly scaled to reflect the primary side input power used in these experiments. A color-mapped graphical representation of the resulting SAR is provided in Fig. 1. The transmitter coil was constructed with a 2-in diameter and ten turns. In two-dimensional simulation, it is represented as two point sources of opposite polarity and is positioned, as indicated in Fig. 1, above the left eye at a location consistent with attachment to a pair of framed reading glasses. The truncated head/eye model is surrounded with 50 perfectly matched layers (PMLs) and then excited with the $\vec{H}$-field sourced from the two-dimensional coil.

Results in Fig. 1 show the power levels, which are scaled to mW/kg and are provided in $\log_{10}$ scale for best viewing with the linear scale added for reference. The SAR distribution shows that the right eye receives more deposited power than the targeted left eye containing the prosthesis. The major reason for the location of this peak SAR in the right eye is the much higher conductivity of the eye humor with respect to other organs, such as cartilage, bone, or skin. The eye with the prosthesis is exposed to minimal electric field (electric field on the axis of the coil is ideally zero), while the largest electric field is found on the sides of the coil. Thus, the opposite eye is exposed to large electric fields compared to organs normal to the axis of the coil. Considering the higher conductivity of the eye humor, this results in relatively high SAR compared to other organs.

III. INFLUENCE OF CHOROIDAL BLOOD FLOW ON OCULAR TEMPERATURE

Studies have revealed a relation between damage to the photoreceptor layer of the retina and ocular temperature [3], [4]. Anterior to the human retina's photoreceptor layer and to the pigmented epithelium lies the choroid, which is a vascularized layer supplying blood to the outer retina. The blood circulation density to the outer retina by way of the choroid is known to be higher than in any other bodily tissue [5], [6]. In fact, the blood flow exceeds the oxygenation needs of the outer retina and the retinal pigment epithelium [5], [6]. It is proposed that the high blood flow from the choroidal layer facilitates the regulation of retinal temperature, which would otherwise increase in the outer retina during the phototransduction of incident light and absorption in the epithelium of excess light energy [7]. Experiments
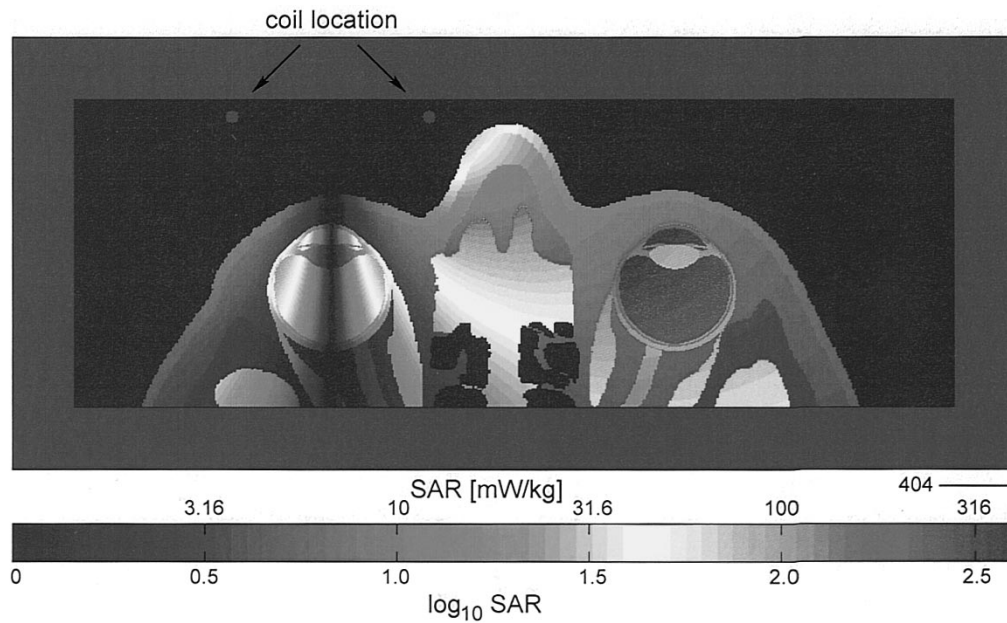
Fig. 1.   Specific absorption rate in log scale at 2-MHz irradiation for 2-A coil current.

revealed that less energy from incident light was necessary in dead animals than in living animals to incur retinal damage [5]. Furthermore, reducing blood flow in living animals also encouraged retinal damage from light energy. Other studies revealed a type of closed-loop neural feedback in which increased energy from incident light produced an increase in choroidal blood flow [8], [9].

In order to gain insight into the influence of choroidal blood flow on ocular cooling, numerical simulations are conducted to compare thermal results first assuming no choroidal blood flow in the head/eye model of Part I, Fig. 8, and subsequently with blood flow modeled. Under both assumptions, the choroid is not considered blood, but is instead identified as an independent, unique tissue type. However, because it is heavily vascularized, it is modeled with the same dielectric and thermal properties and mass density of blood.

IV. THERMAL SIMULATIONS IN THE ABSENCE OF CHOROIDAL BLOOD FLOW

We first consider the absence of choroidal blood flow wherein the temperature of the choroidal tissue is allowed to rise as dictated by the bioheat equation, as any other tissue type would when exposed to heat. Note that the retina is assigned a high blood perfusion constant in Part I, Table IV, wherein the source of this blood is the adjacent choroidal tissue. Thus, we impose the additional constraint that the parameter of T_b occurring in the bioheat equation when evaluating retinal temperature will be replaced with the computed temperature of the choroid and will not be considered fixed at $37\,^{\circ}$C as is the case for other tissues, which are perfused with flowing blood. Thus, we consider a fixed blood temperature $T_b = 37\,^{\circ}$C for all perfused tissues except retina and a variable blood temperature $T_{\text{choroid}} \neq T_b$, in lieu of the retina. The cooling term in the bioheat equation will be $-B(T - T_b)$ for nonretinal tissue and $-B(T - T_{\text{choroid}})$ for retina.
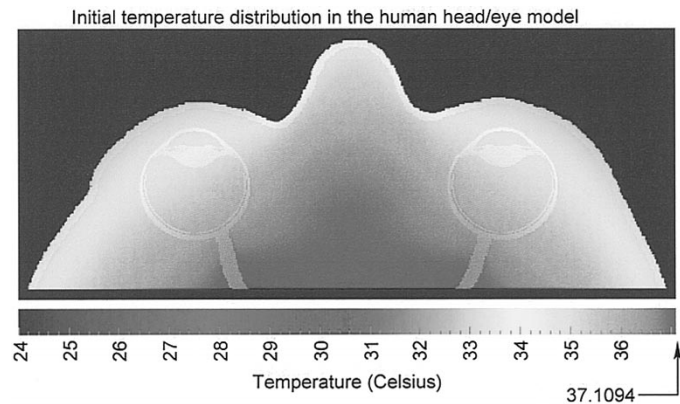

Fig. 2.   Initial temperature distribution (anterior portion) in the human head/eye model in the absence of choroidal blood flow and with no excitation from SAR or from the stimulator IC.

A. Initial Temperature Distribution

As we are interested in the temperature increase above the natural temperature distribution, it is necessary to first simulate thermal spread in the head/eye model of Part I, Fig. 7, beginning at an initial assumed air temperature of $24\,^{\circ}$C, while devoid of the influence of SAR and of the implanted IC. The results of this simulation appear consistent with expectations of the natural temperature distribution in the human head. A peak temperature of $37.2857\,^{\circ}$C occurs within the brain due to the high basal metabolism associated with white and gray matter as seen in Part I, Table IV. Cooler temperatures occur near the interface between the head model and the surrounding air where thermal convection occurs.

The anterior portion of the initial temperature distribution corresponding to the truncated head/eye model of Part I, Fig. 8, is then isolated (Fig. 2) to provide a starting point for predicting thermal increase above the natural temperature distribution due to SAR and the implanted microchip. In this front portion of
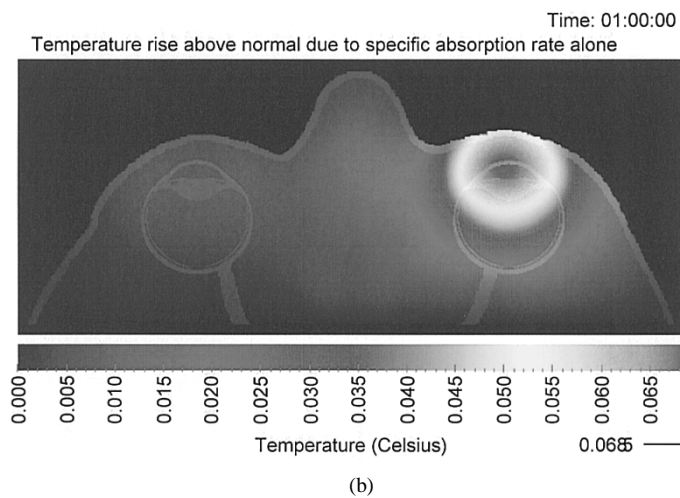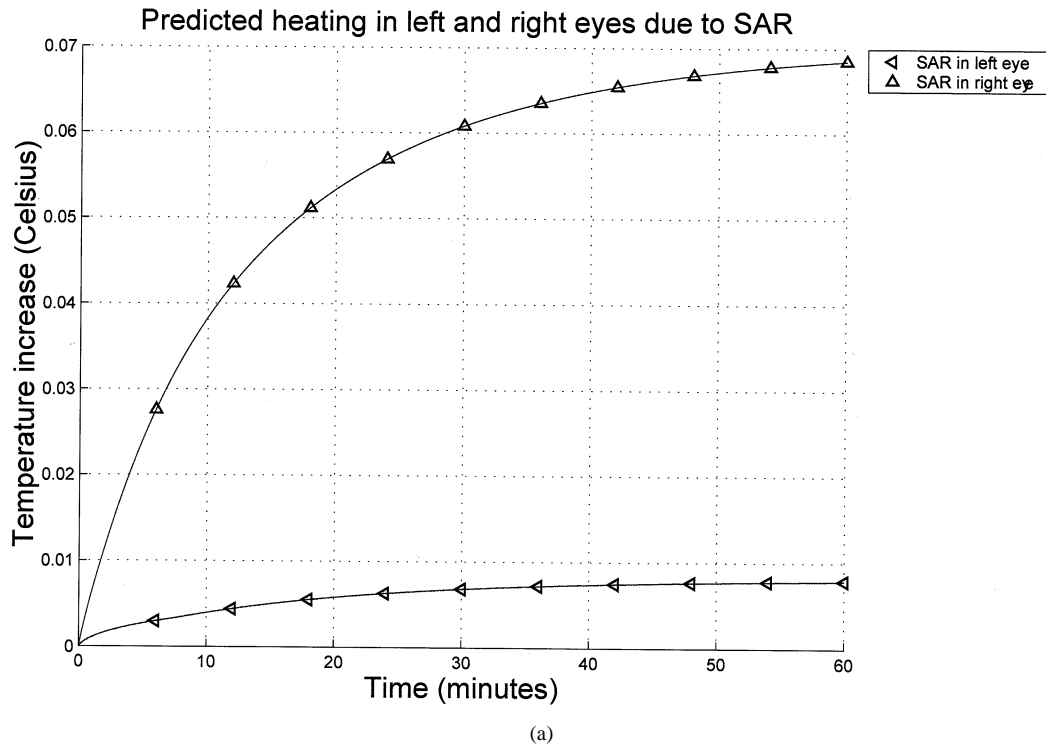
(a)

(b)

Fig. 3. Predicted ocular heating in the head/eye model due to SAR in the absence of choroidal blood flow. (a) Temperature increase versus time. (b) Steady-state distribution after 60 min.

the head model, a peak temperature of 37.1094 °C occurs in the brain.

B. Temperature Increase Due to SAR

A thermal simulation predicting the temperature increase arising from the SAR of Fig. 1 applied to the head/eye model of Part I, Fig. 8, is run with a simulated time coverage of one hour. At the end of one hour of simulated time, the peak temperature rise in the right eye has converged to a value of 0.0685 °C and the rate of increase has diminished to approximately 10^{-7} °C when monitored at 0.5-s intervals.

A plot of temperature increase over time due to SAR for the left and right eyes is provided in Fig. 3(a). The vertical axis represents the increase above the initial temperature distribution encountered over each eye. The SAR distribution of Fig. 1 indicates that most of the power is deposited in the right eye despite targeting the stimulator IC in the left eye, owing to the $\vec{E}$-field distribution associated with the $\vec{H}$-field sourced from the primary coil. Accordingly, the peak thermal increase of 0.0685 °C also occurs in the right eye. Note that the temperature rise in each eye asymptotically approaches steady state as heat continues to spread beyond the eyes and into the surrounding head tissues.

A color-mapped graphical plot of the steady-state temperature distribution resulting from the SAR of Fig. 1 is provided in Fig. 3(b). The maximum temperature increase of 0.0685 °C is indicated by the red area near the lens of the right eye. Once again, this is consistent with the location of the SAR maximum from Fig. 1.
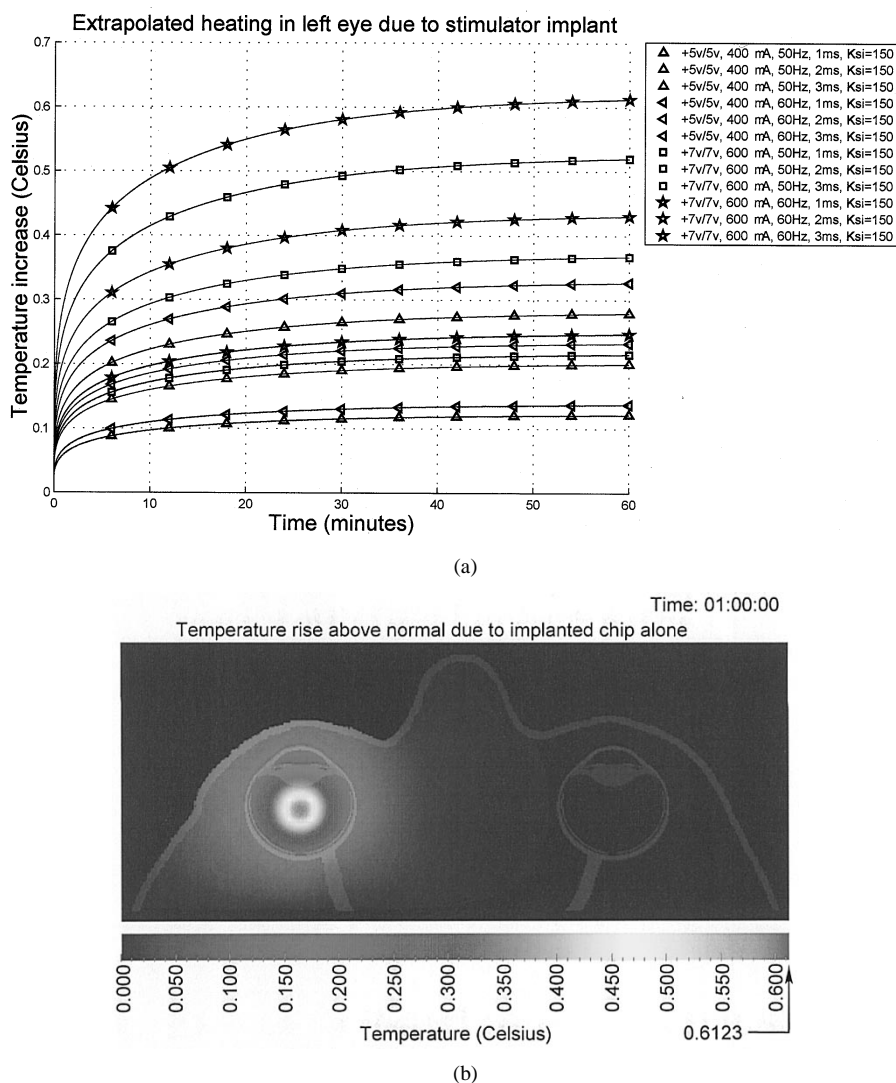
(a)

(b)

Fig. 4. Predicted ocular heating in the head/eye model due to stimulator implant power in the absence of choroidal blood flow. (a) Temperature increase versus time. (b) Steady-state distribution after 60 min.

C. Temperature Increase Due to Power Dissipation in the Implanted Stimulator IC

The stimulator power estimates of Part I Table II, acquired from *Hspice* simulation have been passed to the thermal numerical method developed in Part I, Section II, in order to predict ocular heating. These values correspond to $P_{\text{chip(3-D)}}$ and are used to compute $P_{\text{chip(2-D)}}^{(\text{density})}(i,j)$ in Part I, (3), according to $\underline{(\text{discrete})}$ derivation in Part I, Section IV. A separate thermal simulation has been conducted for each of the 12 variations in biphasic stimulus currents. As with the simulations of thermal increase due to SAR, the initial temperature distribution of Fig. 2 is assumed at the start of each simulation.

A plot of temperature increase in the left eye over time for the 12 stimulation cases is provided in Fig. 4(a). The vertical axis represents the temperature increase of the midvitreous above the initial temperature distribution for the left eye of Part I, Fig. 8, in which the stimulator IC is modeled. Notice again the asymptotic convergence of temperature rise in the left eye occurring for each power scenario, as heat spreads beyond the confines of the left eye.

A color-mapped graphical plot of the predicted steady-state temperature distribution arising from operation of the stimulator IC is provided in Fig. 4(b), corresponding to the expected worst case power dissipation $P_{\text{chip(3-D)}} = 46.4672\,\text{mW}$ from Part I, Table II. A temperature increase of $0.6123\,°\text{C}$ is indicated above the region of the IC in the left eye. At the surface of the retina, the temperature increase appears to be near 0.2–$0.25\,°\text{C}$.

V. THERMAL SIMULATIONS IN THE PRESENCE OF CHOROIDAL BLOOD FLOW

Since the blood flow rate is considered to vary with incident light energy [8], [9], the heat dissipating influence of flowing blood is modeled by holding the choroidal temperature at $T_b = 37\,°\text{C}$, thereby assuming ideally an "infinite" blood flow. In the biological system, the blood is expected to increase above $T_b = 37\,°\text{C}$ as it carries away heat absorbed in the outer retina and pigmented epithelium. But as it quickly circulates and is replaced by fresh blood, we assume that a fixed choroidal temperature of $T_{\text{choroid}} = T_b = 37\,°\text{C}$ in the head/eye model of Part I, Fig. 8, closely approximates the true response of the choroid.
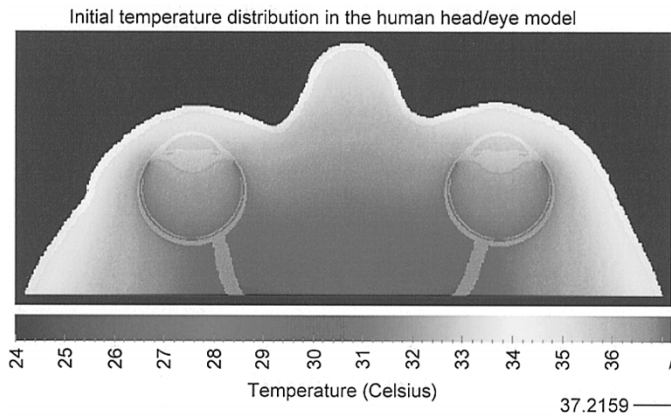
Fig. 5. Initial temperature distribution (anterior portion) in the human head/eye model in the presence of choroidal blood flow and with no excitation from SAR or from the stimulator IC.

A. Initial Temperature Distribution

In Section IV-A, the initial steady-state temperature distribution in the absence of choroidal blood flow was computed as a starting point for simulations predicting thermal increase. Similarly, a new initial distribution is computed in the presence of choroidal blood flow. Once again, this is obtained by assuming a fixed choroidal blood temperature of $T_b = 37\,°C$ and is computed beginning with an air temperature of $24\,°C$ and devoid of the influence of SAR and the implant IC.

The anterior portion of the initial temperature distribution corresponding to the truncated head/eye model of Part I, Fig. 8, is again isolated from the initial distribution as shown in Fig. 5. This new initial temperature distribution clearly highlights the choroidal blood flow now accounted for in thermal simulation, as can be seen in the region posterior to the retina in both eyes as compared with the same areas in Fig. 2 where choroidal blood flow was not included. Thus, this new truncated initial distribution will serve to initialize the thermal simulations of SAR and of the implant IC in the context of blood flow in the choroid. A peak temperature of $37.2159\,°C$ occurs in the anterior portion of the initial temperature distribution, resulting from a forced choroidal blood temperature of $T_b = 37\,°C$. This forced blood temperature in conjunction with heating from the brain with its high basal metabolism results in a peak temperature within the region slightly in excess of the $37.1094\,°C$ encountered in Fig. 2.

B. Temperature Increase Due to SAR

Under the assumption of fixed choroidal temperature, a thermal simulation predicting the temperature increase arising from the SAR of Fig. 1 is again run with a simulated time coverage of one hour. After one hour of simulated time, the peak temperature rise in the right eye has converged to a value of $0.0479\,°C$.

A plot of temperature increase over time due to SAR for the left and right eyes is provided in Fig. 6(a). In contrast to the curves of Fig. 3, the temperature increases for both eyes appear to reach steady state around 35–40 min. The reason for this rapid convergence is that the fixed blood of $37\,°C$ in the eyes prevents heat from spreading across the choroid as can be clearly seen

in the color-mapped graphical plot of the steady-state temperature distribution resulting from the SAR of Fig. 1 as provided in Fig. 6(b). This is in strong contrast to the situation present in Fig. 3, where the diffusion of heat does occur across the choroid where its temperature is not forced at $37\,°C$. The maximum temperature increase of $0.0479\,°C$ is indicated by the red area concentrated in the aqueous humor of the anterior chamber forward of the lens. The fact that the isotherms over the right eye of Fig. 6(b) do not cross over the choroid as they do in Fig. 3(b) indicates that the choroid is acting to provide thermal regulation. This is no longer evident near the vitreous base and over the cornea where the SAR-induced heat expands beyond the boundaries of the right eye.

C. Temperature Increase Due to Power Dissipation in the Implanted Stimulator IC

Again under the assumption of fixed choroidal temperature, thermal simulations are once more run for each of the 12 stimulation cases, using microchip power estimates from Part I, Table II, in order to predict ocular heating in the left eye due to the stimulator implant.

A plot of temperature increase in the left eye over time for the 12 stimulation cases is provided in Fig. 7(a). As with the SAR-induced heating in the context of choroidal blood flow, the temperature increases again appear to converge to steady state within 30 min.

A color-mapped graphical plot of the predicted steady-state temperature distribution arising from operation of the stimulator IC is provided in Fig. 7(b), corresponding to the expected worst case power dissipation $P_{chip(3-D)} = 46.4672$ mW from Part I, Table II. Due to the fixed temperature of the choroid, a reduced temperature increase of $0.4349°C$ is now indicated in the region above the IC in the left eye. The temperature increase appears minimal near the surface of the retina. In contrast to Fig. 4(b), where heat from the stimulator IC expands beyond the eye region and into the surrounding head tissues, Fig. 7(b) indicates a larger portion of the heat is localized by the choroid. Only near the anterior of the eye where the choroid ends do we see heat spreading beyond the left eye boundary.

VI. COMPARISON OF THERMAL RESULTS WITH AND WITHOUT CHOROIDAL BLOOD FLOW

The numerical simulations of Sections IV and V clearly indicate the potential benefit that may be afforded to an implantable prosthesis by the blood flow of the choroid. In regards to SAR, notice that the amount of cooling is more prominent in the right eye where the SAR (deposited electromagnetic power) is greater. The temperature in the right eye is lower by $0.0206\,°C$ for a decrease of 30.07%, while the maximum in the left eye is lower by $0.0039\,°C$ for a decrease of 49.37%, as summarized in Table I.

Similar comparisons are provided for ocular heating due to power dissipation in the stimulator IC and take into account the 12 simulated variations in biphasic stimulus currents. In the worst operating conditions considered, corresponding to biphasic stimulus currents of $600\ \mu A$ amplitude at 60-Hz
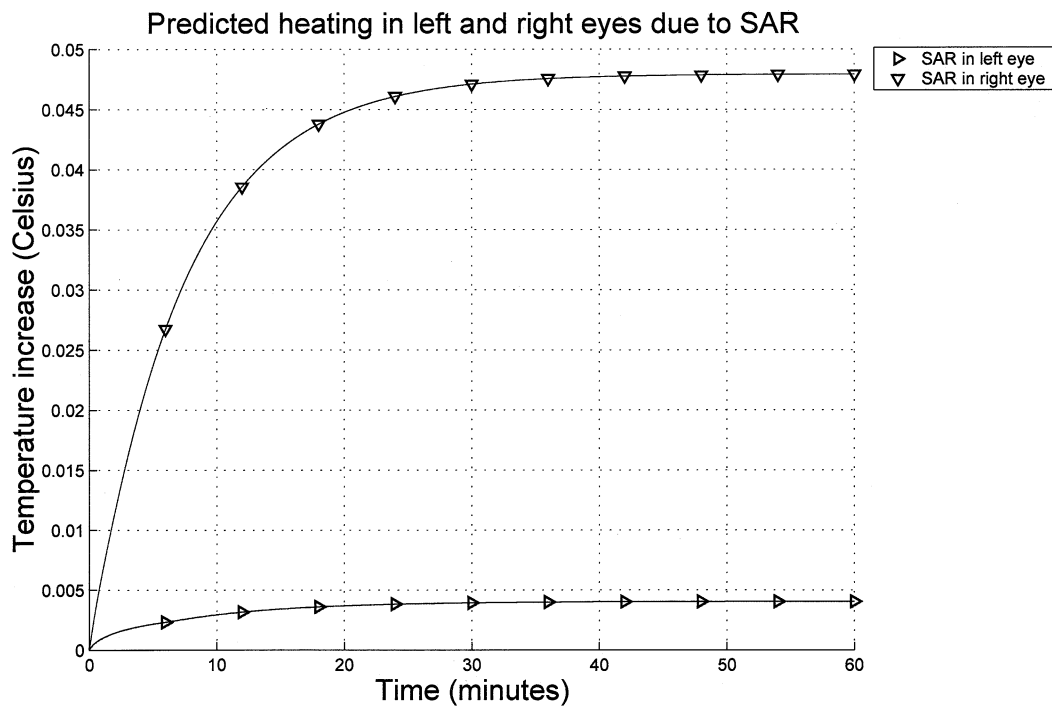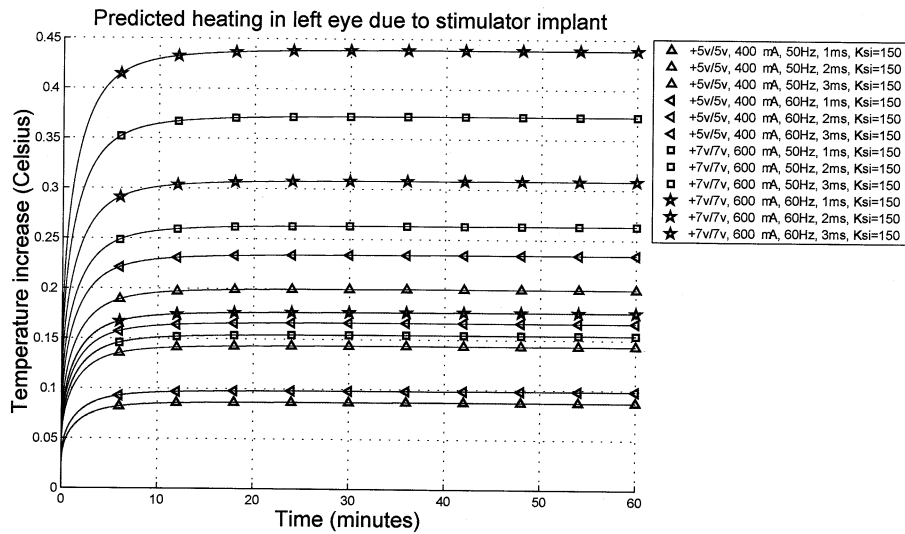
(a)
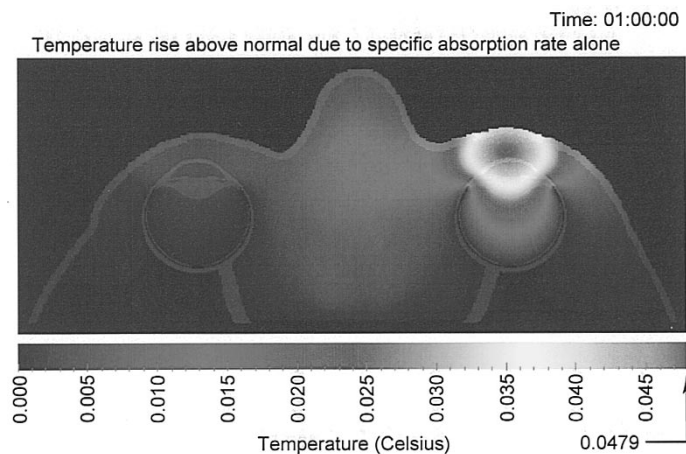
(b)

Fig. 6.   Predicted ocular heating in the head/eye model due to SAR in the presence of choroidal blood flow. (a) Temperature increase versus time. (b) Steady-state distribution after 60 minutes.

repetition rate and 3-ms pulse width, the temperature increase in the midvitreous of the left eye above the chip (external to the chip) while accounting for blood flow in the choroid is lower by 0.1774 °C for a decrease of 28.97% with respect to temperature rise obtained with no blood flow. This comparison for the worst case and the remaining operating conditions considered is summarized in Table II.

A further comparison of the thermal simulation results with and without choroidal blood flow is provided in Fig. 8. Temperature increase in the midvitreous of the left eye above the chip for the 12 operating scenarios is plotted versus stimulator IC power. The upper bounding curve represents a least squares linear fit to the thermal results in the absence of choroidal blood flow, while the lower bounding curve represents a fit to the thermal results in the presence of choroidal blood flow.

The gray-shaded region between the bounding curves represents the uncertainty region, wherein the actual temperature increase associated with the finite yet unknown blood flow rate is expected to occur. Steady-state temperature increase in the midvitreous of the left eye tracks linearly with stimulator power dissipation both in the presence and absence of blood flow. Notice that, as the power dissipation increases, the difference between temperature predictions for the presence and absence of blood flow also increases for corresponding stimulator IC operating conditions.

All the results reported above are relative to a thermal conductivity of bare silicon, and they intend to model the temperature increase induced in the midvitreous of the eye above the chip. However, it should be noted that the actual temperature increases will be strongly dependent upon the composition of the

(a)
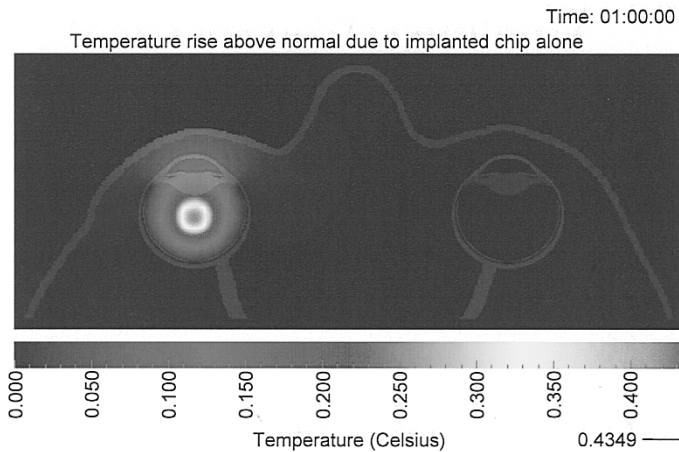
(b)

Fig. 7.   Predicted ocular heating in the head/eye model due to stimulator implant power in the presence of choroidal blood flow. (a) Temperature increase versus time. (b) Steady-state distribution after 60 min.

<div style="display:flex">

TABLE I
TEMPERATURE ELEVATIONS RESULTING FROM THE THERMAL SIMULATION OF SAR, CORRESPONDING TO FIG. 1, IN THE ABSENCE OF CHOROIDAL BLOOD FLOW

Model region[1]	Maximum SAR $\left[\frac{mW}{kg}\right]$	Peak increase above the initial temperature $\Delta T = T - T_0$ [°C]	
		(− blood)[2]	(+ blood)[3]
over left eye	111.9966	0.0079	0.0040
over right eye	404.1180	0.0685	0.0479

TABLE II
TEMPERATURE ELEVATIONS RESULTING FROM THE *HSPICE* SIMULATED POWER DISSIPATION ESTIMATES $P_{\text{chip}(3-D)}$ FROM PART I, TABLE II, IN THE ABSENCE OF CHOROIDAL BLOOD FLOW

V_{dd}, V_{ss} [V_{DC}]	current A [μA]	frame rate $f = \frac{1}{T}$ [Hz]	pulse width W [ms]	Simulated chip power[1] $P_{chip(3D)}$ [mW]	Increase above the initial temperature[2] $\Delta T = T - T_0$ [°C]	
					(−blood)[3]	(+blood)[4]
+5,−5	400	50	1	9.1862	0.1210	0.0860
+5,−5	400	50	2	15.1580	0.1997	0.1419
+5,−5	400	50	3	21.1874	0.2792	0.1983
+5,−5	400	60	1	10.4012	0.1371	0.0974
+5,−5	400	60	2	17.6018	0.2319	0.1648
+5,−5	400	60	3	24.8018	0.3268	0.2321
+7,−7	600	50	1	16.3216	0.2151	0.1528
+7,−7	600	50	2	27.8308	0.3667	0.2605
+7,−7	600	50	3	39.4527	0.5198	0.3693
+7,−7	600	60	1	18.7112	0.2465	0.1751
+7,−7	600	60	2	32.5892	0.4294	0.3050
+7,−7	600	60	3	46.4672	0.6123	0.4349

</div>

implant, and three-dimensional simulations should be employed to characterize these effects.

VII. EXPERIMENTAL VALIDATION

In supplement to the analytical validations of the numerical methods presented in Part I, Section II [10], a further step has been taken to gain additional confidence in the thermal simulation results presented in Section IV and V. Researchers at the University of Southern California (USC) [formerly at Johns Hopkins University (JHU)] have experimentally measured the thermal response to power dissipation introduced into the eyes of dogs [11]. In one of several experiments in this work, 500 mW
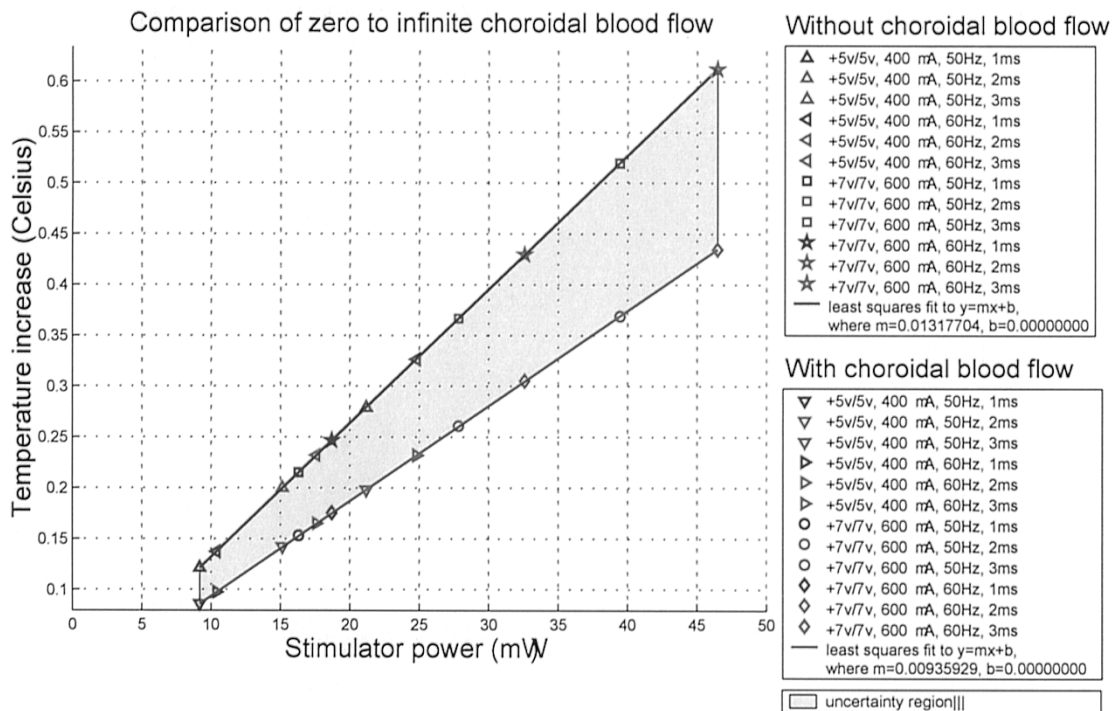
Fig. 8.   A comparison of predicted ocular heating versus stimulator implant power while considering the absence and presence of choroidal blood flow.

of power dissipation introduced intraocularly for a duration of two hours at midvitreous via a ceramic-tipped resistive heating element led to a 2 °C increase in the temperature measured at the retina surface. The simulated thermal elevations encountered in the left eye versus the 12 power dissipations considered for the stimulator IC, as shown in Fig. 8, represent the elevation that occurred in the midvitreous of the eye, above the location of the stimulator IC model in Part I, Fig. 8. In order to correlate these data with this experimental measurement at USC/JHU [11], the simulated thermal elevation encountered at the retina surface is plotted versus the power dissipation in the stimulator IC, as shown in Fig. 9.

The upper line corresponds to the heating at the retinal surface in the absence of any choroidal blood flow. Conversely, the lower line is associated with retina heating where choroidal "infinite" blood flow is maintained. In the latter case, the fixed choroidal temperature of 37 °C prevents the adjacent retina from heating as greatly as in the former case where the choroidal temperature is not held fixed. As such, a maximum simulated temperature elevation of only 0.0038 °C is observed.

Based on the observed linear dependence of retinal heating over the range of power dissipations shown here, extrapolating the 500-mW power dissipation used in the experiments at USC/JHU back down to $P_{\text{chip(3-D)}} = 46.4672$ mW (the highest power dissipation considered for the stimulator IC) would predict a thermal elevation of 0.1859 °C. From the data associated with the case of no choroidal blood flow plotted in Fig. 9, the thermal elevation encountered at the retinal surface for $P_{\text{chip(3-D)}} = 46.4672$ mW is 0.1876 °C. This is in good agreement with the measured value [11]. Although the data were obtained from live eyes with choroidal blood flow, no significant changes were measured when choroidal blood flow was stopped partway through one of the experiments [11].

The lack of any observed variations in recorded temperatures during collection of experimental data appears to indicate that the model with no blood flow is closer to reality than the model with infinite blood flow, meaning that the blood vessels in the choroid are not such to maintain the choroidal temperature at a constant value of 37 °C.

VIII. CONCLUSION

We have presented a numerical study of the thermal increase in the human eye and head associated with the operation of an implantable retinal prosthesis to recover limited sight in blind patients affected by retinitis pigmentosa or age-related macular degeneration. The prosthesis system intends to provide electrical stimulation to existing living ganglion and bipolar cells of the retina using an array of on-chip stimulus circuits and uses inductive telemetry over coils for power and data communication. The demonstration that direct electrical stimulation of retinal ganglion cells can create visual sensation in patients has been shown clinically [12], [13], and patients have been able to recognize English characters and other simple forms when stimulated by a small array of retinal electrodes.

A new two-dimensional 0.25-mm resolution cross-section of the human head has been developed with a novel semiautomatic discretizer to account for the finest anatomical details of the human eye. While a D-H FDTD method with PML absorbing boundary conditions has been used to compute the electromagnetic fields induced in the human head by the external telemetry coil, a discretized version of the bioheat equation accounting for both induced SAR and dissipated power of the implanted microchip has been developed to compute the temperature elevation in the human eye associated with the retinal prosthesis system.
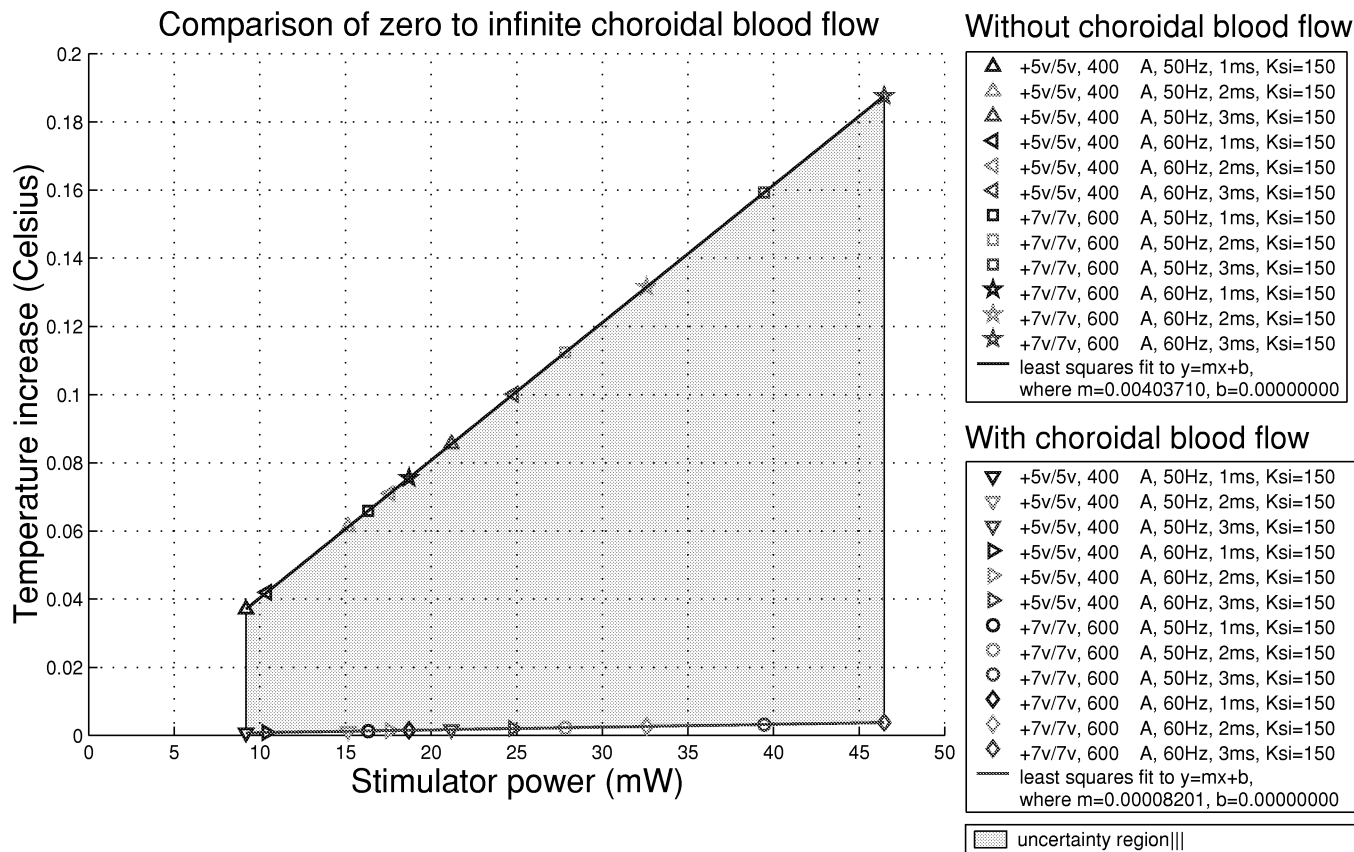
Fig. 9. A comparison of computed ocular heating over the left eye versus power dissipation in the stimulator IC while considering the absence and presence of choroidal blood flow. This heating occurs at the inner retinal surface near the fovea.

We have concluded that in the absence of choroidal blood flow, which corresponds to the case of blood flow rates that are not sufficient to carry away a significant amount of heat, a maximum temperature rise of $0.0685\,^{\circ}\mathrm{C}$ is induced by the external telemetry coil in the eye that does not contain the implanted microchip. Conversely, when considering choroidal blood flow, corresponding to the case of blood flow rates that are such to maintain the temperature of the choroid at a steady $37\,^{\circ}\mathrm{C}$, a reduced maximum rise induced by SAR of $0.0479\,^{\circ}\mathrm{C}$ occurs.

The largest temperature increase associated with the operation of the retinal prosthesis has been shown to be due to the power dissipated by the stimulator IC, which has been evaluated under different operational conditions, corresponding to various degrees of damage of the patient's retina, and different choroidal blood flow assumptions. A temperature rise of $0.6123\,^{\circ}\mathrm{C}$ in the eye with the implant in the absence of blood flow and a reduced increase of $0.4349\,^{\circ}\mathrm{C}$ when accounting for blood flow has been recorded when computing the temperature increase in the midvitreous above the implanted microchip. It should be noted, however, that temperature increase induced on the retina, the most delicate organ in the human eye, was lower than $0.2\,^{\circ}\mathrm{C}$ when the implanted microchip was collocated in the center of the eyeball.

Computed results appear to parallel recent experimental results in animals, especially for the case of absence of choroidal blood flow. However, we should note that the proposed two-dimensional methods and models can characterize the temperature increase in the midvitreous above the implanted microchip, which can be lower than the actual maximum temperature on the surface of the microchip itself.

A complete and accurate characterization of the temperature distribution on the chip and in the eye can be achieved by using three-dimensional modeling. In this case, the disadvantages are the extremely large computer memory requirements and computational times necessary to perform simulations characterized by a suitable resolution of the computational mesh.

REFERENCES

[1] S. C. DeMarco, S. M. Clements, and W. Liu, "A 60 channel implantable neuro-stimulator for an epi-retinal visual prosthesis,", unpublished.
[2] P. R. Troyk and M. A. K. Schwan, "Closed-loop class E transcutaneous power and data link for microimplants," *IEEE Trans. Biomed. Eng.*, vol. 39, pp. 589–599, June 1992.
[3] W. K. Noell, V. S. Walker, and B. S. Kang *et al.*, "Retinal damage by light in rats," *Inv. Ophthalmol. Visual Sci.*, vol. 5, p. 450, 1966.
[4] E. Friedman and T. Kuwubara, "The retinal pigment epithelium: IV. The damaging effects of radiant energy," *Arch. Ophthalmol.*, vol. 80, pp. 265–279, 1968.
[5] L. M. Parver, C. Auker, and D. O. Carpenter, "Choroidal blood flow as a heat dissipating mechanism in the macula," *Amer. J. Ophthalmol.*, vol. 89, pp. 641–646, 1980.
[6] J. T. Ernest, "Choroidal circulation," in *Retina*, 2 ed, S. J. Ryan, Ed. St. Louis, MO: Mosby-Yearbook, 1994, vol. 1, Basic Science and Inherited Retina Disease, pp. 76–80.
[7] P. W. V.Peter W. V. Gurney, "Is our 'inverted' retina really a 'bad design'?," *Creation Ex Nihilo*, vol. 13, no. 1, 1999.
[8] L. M. Parver, C. Auker, and D. O. Carpenter, "Choroidal blood flow: III. Reflexive control in the human," *Arch. Ophthalmol.*, vol. 101, p. 1604, 1983.
[9] L. M. Parver, "Temperature modulating action of choroidal blood flow," *Eye*, vol. 5, p. 181, 1991.

[10] F. Bardati, G. Gerosa, and P. Lampariello, "Temperature distribution in simulated living tissues irradiated electromagnetically," *Alta Frequenza*, vol. XLIX, no. 2, pp. 61–67, 1980.

[11] D. V. Piyathaisere, E. Margalit, S. J. Chen, J. S. Shyu, S. A. D'Anna, J. D. Weiland, R. R. Grebe, L. Grebe, G. Fujii, S. Y. Kim, R. J. Greenberg Jr., E. De Juan, and M. S. Humayun, "Heat effects on the retina," *Ophthal. Surgery Lasers*, July 3, 2001.

[12] M. S. Humayun, E. De Juan Jr., G. Dagnelie, R. J. Greenberg, R. H. Propst, and H. Phillips, "Visual perception elicited by electrical stimulation of the retina in blind humans," *Arch. Ophthalmol.*, vol. 114, pp. 40–46, 1996.

[13] M. S. Humayun, E. De Juan Jr., J. D. Weiland, G. Dagnelie, S. Katona, R. Greenberg, and S. Suzuki, "Pattern electrical stimulation of the human retina," *Vision Res.*, vol. 39, pp. 2569–2576, 1999.
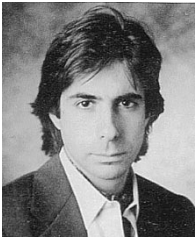
Gianluca Lazzi (S'94–M'95–SM'99) was born in Rome, Italy, on April 25, 1970. He received the Dr.Eng. degree in electronics from the University of Rome La Sapienza, Rome, Italy, in 1994 and the Ph.D. degree in electrical engineering from the University of Utah, Salt Lake City, in 1998.

He has been a Consultant for several companies (1988–1994), Visiting Researcher at the Italian National Board for New Technologies, Energy, and Environment (ENEA) (1994), Visiting Researcher at the University of Rome La Sapienza (1994–1995), and Research Associate (1995–1998) and Research Assistant Professor (1998–1999) at the University of Utah. He is presently an Assistant Professor at the Department of Electrical and Computer Engineering, North Carolina State University, Raleigh. He is author or coauthor of more than 70 international journal articles or conference presentations on FDTD modeling, dosimetry, and bioelectromagnetics.

Dr. Lazzi received a 2001 NSF CAREER Award, a 2001 Whitaker Foundation Biomedical Engineering Grant for Young Investigators, a 1996 International Union of Radio Science (URSI) Young Scientist Award, and the 1996 Curtis Carl Johnson Memorial Award for the best student paper presented at the eighteenth annual technical meeting of the Bioelectromagnetics Society. He is an Associate Editor for the IEEE ANTENNAS AND WIRELESS PROPAGATION LETTERS. He is listed in *Who's Who in the World, Who's Who in America, Who's Who in Science and Engineering, Dictionary of International Biographies,* and *2000 Outstanding Scientists of the 20th Century.*

Stephen C. DeMarco was born in Fairmont, WV, in 1971. He received the B.S. *(summa cum laude)* and M.S. degrees in computer engineering from North Carolina State University, Raleigh, in 1994 and 1996, respectively, where he is currently pursuing the Ph.D. degree in electrical engineering.

His research is in the areas of analog/digital/mixed-mode circuit design, VLSI, FPGAs, and computer vision/image-processing applicable to retina prosthesis development.

Wentai Liu (S'78–M'81–SM'93) received the Ph.D. degree in computer engineering from the University of Michigan at Ann Arbor in 1983.

He has been since 1983 on the Faculty of North Carolina State University, Raleigh, where he is currently the Alcoa Professor of Electrical and Computer Engineering. His research focuses on retinal prosthesis to restore eyesight for the blind, molecular electronics, analog and digital VLSI design and CAD, phase-locked-loop, noise characterization and modeling, timing/clock optimization, high-speed transceiver for communication network, digital CMOS camera, telemetry design, and microelectronic sensor design.

Prof. Liu received an IEEE Outstanding Paper Award in 1986 and the Alcoa Foundation's Distinguished Engineering Research Award in 1999.

James D. Weiland (S'92–M'99) received the B.S. degree, the M.S. degree in biomedical engineering and electrical engineering, and the Ph.D. degree in biomedical engineering from the University of Michigan, Ann Arbor, in 1988, 1993, 1995, and 1997, respectively.

From 1997 to 2001, he was with the Wilmer Ophthalmological Institute, Johns Hopkins University, first as a Postdoctoral Fellow and then as an Assistant Professor. In 2001, he became an Assistant Professor in the Department of Ophthalmology, University of Southern California Keck School of Medicine, Doheny Eye Institute, Los Angeles, CA. His interests include retinal prostheses, electrode technology, visual evoked responses, and implantable electrical systems.

Dr. Weiland is a member of the IEEE EMBS, the Biomedical Engineering Society, and the Association for Research in Vision and Ophthalmology.
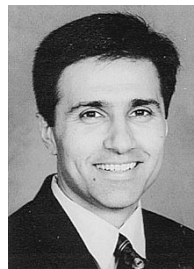
Mark S. Humayun (M'97) received the M.D. degree from Duke University, Durham, NC, in 1989 and the Ph.D. degree in biomedical engineering from the University of North Carolina, Chapel Hill, in 1993.

He has been Assistant and Associate Professor at the Department of Ophthalmology, Johns Hopkins Hospital, Baltimore, MD. He is currently a Professor in the Department of Ophthalmology, University of Southern California Keck School of Medicine, Doheny Eye Institute, Los Angeles, CA.